https://doi.org/10.5194/bg-2019-212
Preprint. Discussion started: 14 June 2019

Biogeosciences Discussions

Global biosphere–climate interaction: a multi-scale appraisal of observations and models

Jeroen Claessen[1], Annalisa Molini[2], Brecht Martens[1], Matteo Detto[3], Matthias Demuzere[1,4], and Diego Miralles[1]

[1]Laboratory of Hydrology and Water Management, Department of Environment, Ghent University, Ghent, Belgium
[2]Masdar Institute, Khalifa University of Science and Technology, Abu Dhabi, United Arab Emirates
[3]Department of Ecology and Evolutionary Biology, Princeton University, Princeton, United States of America
[4]Department of Geography, Ruhr-University Bochum, Bochum, Germany

Correspondence: Jeroen Claessen (Jeroen.Claessen@UGent.be)

Abstract. Improving the skill of Earth System Models (ESMs) in representing climate–vegetation interactions is crucial to enhance our predictions of future climate and ecosystem functioning. Therefore, ESMs need to correctly simulate the impact of climate on vegetation, but likewise, feedbacks of vegetation on climate must be adequately represented. However, model predictions at large spatial scales remain subjected to large uncertainties, mostly due to the lack of observational patterns to benchmark them. Here, the bi-directional nature of climate-vegetation interactions is explored across multiple temporal scales by adopting a spectral Granger causality framework that allows identifying potentially co-dependent variables. Results based on global and multi-decadal records of remotely-sensed leaf area index (LAI) and observed atmospheric data show that the climate control on vegetation variability increases with longer temporal scales, being higher at inter-annual than multi-month scales. The phenological cycle in energy-driven latitudes is mainly controlled by radiation, while in (semi-)arid regimes precipitation variability dominates at all temporal scales. However, at inter-annual scales, the control of water availability gradually becomes more wide-spread than that of energy constraints. The observational results are used as a benchmark to evaluate ESM simulations from the Coupled Model Intercomparison Project Phase 5 (CMIP5). Findings indicate a tendency of ESMs to over-represent the climate control on LAI dynamics, and a particular overestimation of the dominance of precipitation in arid and semi-arid regions. Analogously, CMIP5 models overestimate the control of air temperature on forest seasonal phenology. Overall, climate impacts on LAI are found to be stronger than the feedbacks of LAI on climate in both observations and models, arguably due to the local character of the analysis that does not allow for the identification of downwind or remote vegetation feedbacks. Nonetheless, wide-spread effects of LAI variability on radiation are observed over the northern latitudes, presumably related to albedo changes, which are well-captured by the CMIP5 models. Overall, our experiments emphasise the potential of benchmarking the representation of particular interactions in online ESMs using causal statistics in combination with observational data, as opposed to the more conventional evaluation of the magnitude and dynamics of individual variables.

https://doi.org/10.5194/bg-2019-212
Preprint. Discussion started: 14 June 2019

Biogeosciences Discussions Open Access EGU

1 Introduction

The biosphere is a key actor in the global carbon and water cycles, mainly through its impact on the energy balance at the Earth's surface and the chemistry of the atmosphere (McPherson, 2007; Pearson et al., 2013; Le Quéré et al., 2018). Long-term patterns in temperature, incoming radiation and water availability strongly control the global distribution of biomes, while vegetation in turn alters climate via a series of local and remote feedbacks (Kottek et al., 2006; Bonan, 2008). In boreal regions, for example, vegetation is thought to preferentially warm the atmosphere (positive feedback) by lowering the surface albedo, while in tropical regions, it is expected to have a local net cooling effect (negative feedback), mainly due to high transpiration (Bonan, 2008; Forzieri et al., 2017). Furthermore, our biosphere also provides a strong negative feedback to the the global carbon cycle by acting as a carbon sink (Schimel et al., 2015). This strong regulating power of vegetation in our Earth system indicates the need to properly incorporate biosphere–climate interactions in the models used to predict changes in terrestrial ecosystems and future climate (Piao et al., 2013; Pachauri et al., 2014; Le Quéré et al., 2018). As Earth System Models (ESMs) are expected to imperfectly capture the sensitivity of vegetation to climate, and vice versa (Green et al., 2017), different approaches have been followed to objectively evaluate their skill in representing these interactions (Randerson et al., 2009; Weiss et al., 2012; Murray-Tortarolo et al., 2013; Alessandri et al., 2017; Forzieri et al., 2018). Most of these efforts focus on the evaluation of the magnitude and dynamics of individual variables (such as leaf area index, LAI, and gross primary production, GPP), rather than on the representation of particular inter-variable sensitivities.

Nonetheless, a first and necessary requirement towards improving the predictive skill of ESMs is the availability of data that can be used as reference. Satellite observations of our biosphere, hydrosphere and atmosphere are now widely available, providing multi-decadal records of climatological and environmental variables at global scale that can be used as benchmark. Several studies have already focused on identifying short- and long-term global impacts of climate on vegetation using observational data, mostly from satellites (Nemani et al., 2003; Zhao and Running, 2010; Forkel et al., 2014; De Keersmaecker et al., 2015; Wu et al., 2015; Seddon et al., 2016; Papagiannopoulou et al., 2017b). Nonetheless, studies focusing on how the dominant interactions vary as a function of temporal scale (e.g., monthly, seasonally and inter-annually) are still lacking, and so is the evaluation of this inter-scale variability in ESMs. In a recent example, Papagiannopoulou et al. (2017b) focused on evaluating multi-month vegetation variability in response to local climate, using a non-linear Granger causality framework. They showed that water availability and precipitation patterns primarily drive vegetation anomalies at monthly scales in more than 60% of the vegetated land. While this study evaluated the ecosystem response based on optical remote sensing indices, the influence of climate on terrestrial ecosystem carbon fluxes has also been intensively explored in recent years, with apparent contradictions in the findings regarding the importance of water availability for inter-annual biosphere dynamics (Jung et al., 2017; Humphrey et al., 2018; Green et al., 2019; Stocker et al., 2019). In addition, most studies to date have either attributed the covariance of vegetation and climate dynamics to the role of atmospheric processes driving biosphere variability (e.g., Nemani et al., 2003; Zhao and Running, 2010; Forkel et al., 2014; De Keersmaecker et al., 2015; Wu et al., 2015; Papagiannopoulou et al., 2017b), or to the opposite processes, i.e. the feedbacks of vegetation on climate (e.g., Forzieri et al., 2017; Zeng et al., 2017). To the authors knowledge, the study by Green et al. (2017) is the only exception in which the causal directionality of

https://doi.org/10.5194/bg-2019-212
Preprint. Discussion started: 14 June 2019

vegetation–climate interactions has been formally disentangled at global scales. In this study, a linear Granger causality approach was used to successfully unravel impacts and feedbacks between biosphere and climate at multi-month scales. However, the traditional Granger causality framework is unsuited to identify which interactions dominate at different temporal scales, thus to differentiate between the dominant causes and effects at multi-month, seasonal and inter-annual scales (Detto et al., 2012).

Here, we investigate climate–vegetation interactions over the global domain using an innovative variant of Granger causality, referred to as Conditional Spectral Granger Causality (CSGC) – see Detto et al. (2012). CSGC relies on transforming time series from the time domain into a time–frequency space using the continuous wavelet transform, enabling the simultaneous analysis of interactions that are active at different temporal scales, from e.g. monthly to inter-annual. In addition, this technique allows for evaluating the contribution of any variable while conditioning on the others, and, because CSGC can cope with lagged responses, it enables the assessment of bi-directional interactions (Dhamala et al., 2008; Detto et al., 2012; see Sect. 2.2). The latter implies that the vegetation feedback on climate can be quantified separately from the climate impact on vegetation. In this study, CSGC is first applied to satellite observations to reveal useful insights regarding the global, multi-scale, bi-directional interaction between vegetation dynamics and local climate (Sect. 3.1 and 3.3). Next, to benchmark the ESM representation of these biosphere–climate interactions, the approach is replicated using the outcome from online simulations from the Coupled Model Intercomparison Project Phase 5 (CMIP5) models (Taylor et al., 2012; see Sect. 3.2 and 3.3). By comparing the observational and model-based results, areas where certain processes and inter-variable sensitivities may be incorrectly represented in ESMs are identified.

2 Data and methods

2.1 Data

Multiple satellite-based datasets are used to evaluate the representation of climate–vegetation interactions in ESMs. The focus is on the key climatic drivers of vegetation growth, here assumed to be precipitation, net radiation and air temperature, consistent with previous studies (Nemani et al., 2003; Seddon et al., 2016; Jung et al., 2017; Papagiannopoulou et al., 2017b). Vegetation dynamics are diagnosed using LAI; in the following, when vegetation (state) is mentioned, the latter refers to LAI unless stated otherwise. All datasets have global coverage, are processed into $0.5°$ spatial resolution via bilinear interpolation, and are averaged to monthly values prior to the application of CSGC.

2.1.1 Observational data

Observations of LAI come from the Global Inventory Modelling and Mapping Studies 3rd generation (GIMMS3g; Zhu et al., 2013). Bimonthly LAI data at $1/12°$ spatial resolution is produced using a neural network between GIMMS3g Normalised Difference Vegetation Index (NDVI) and LAI from the Moderate Resolution Imaging Spectroradiometer (MODIS). The final dataset covers the period July 1981 – December 2015. Climate data is obtained from the Climate Research Unit - National

https://doi.org/10.5194/bg-2019-212
Preprint. Discussion started: 14 June 2019

Centers for Environmental Prediction (CRU-NCEP) version 7 (Viovy, 2018). CRU-NCEP provides atmospheric data obtained through merging the CRU TS3.2 observations and NCEP reanalysis data, resulting in a $0.5°$ product, available from 1901 up to 2016. Finally, for the comparison of the results between observations and models, the International Geosphere-Biosphere Program (IGBP) land cover classification (Loveland and Belward, 1997) is used to determine biome-specific behaviours. At a biome-level, the mean observed and modelled interactions are calculated, and the range in ESM results is determined. These biomes include mixed forests (MF), deciduous broadleaf forest (DBF), deciduous needleleaf forest (DNF), evergreen broadleaf forest (EBF), evergreen needleleaf forest (ENF), barren or sparsely vegetated (BSV), cropland or natural vegetation mosaic (CNVM), croplands (C), grasslands (G), savannas (S), woody savannas (WS), and open shrublands (OS).

2.1.2 Earth System Model data

A selection ESMs, i.e. Hadley Global Environment Model 2 - Earth System (HadGEM2-ES; Collins et al., 2011), Institut Pierre Simon Laplace - Component Models 5 - Medium Resolution (IPSL-CM5A-MR; Dufresne et al., 2013), Norwegian Earth System Model 1 - Medium Resolution (NorESM1-M; Bentsen et al., 2013), and Community Climate System Model 4 (CCSM4; Gent et al., 2011), from the Coupled Model Intercomparison Project Phase 5 (CMIP5; Taylor et al., 2012) is assessed in their representation of climate–vegetation interactions. Using the historical input climate data, one realisation was used for each model to simulate vegetation dynamics, resulting in a monthly time series of LAI. Due to the discontinuation of historical simulations in 2005, the overlap with the observational record is limited to 24 complete years. To enhance the robustness of the results, the analysis period considers the entire 1956-2005 in the case of ESMs, under the assumption that the sensitivities are stationary (see e.g. Green et al., 2017). Nonetheless, we acknowledge that the non-stationarity associated with changes in land use and land cover may induce divergences between the observation and model results.

2.2 Methods

Multi-frequency interactions between climate and vegetation are here explored using CSGC. To describe the method comprehensively, we first introduce the Granger causality in its classical formulation (parametric in the time domain; Sect 2.2.1), followed by the derivation of its spectral counterpart (non-parametric in the time-frequency domain; Sect. 2.2.2 and 2.2.3).

2.2.1 Granger Causality: Time domain formulation

According to Granger (1969), causality can be inferred if a predictor X ($[x_1, x_2 ... x_{n-1}, x_n]$), with n the number of time steps, contains information in past terms that aids the prediction of a target variable Y ($[y_1, y_2 ... y_{n-1}, y_n]$), while this information is not contained in any other predictor or past values of the target variable itself. To assess the predictive power of X on Y, the self-explanatory power of Y, i.e. the autocorrelation, has to be determined first, so it can later be factored out. At time t, the auto-predictive power of Y can be calculated with the following univariate autoregressive equation:

$$y_t = \sum_{i=1}^{m} a_i y_{t-i} + \epsilon_t \quad (1)$$

https://doi.org/10.5194/bg-2019-212
Preprint. Discussion started: 14 June 2019

where m defines the order of the autoregressive model (with $m \leq n$), i is the time lag, a_i are the coefficients describing the linear interaction between different time steps, and ϵ_t is the prediction error.

The predictive power of X on Y can be assessed through construction of a second autoregressive model, containing a term capturing the contribution of X, given by:

$$y_t = \sum_{i=1}^{m} a_i y_{t-i} + \sum_{i=1}^{m} b_i x_{t-i} + \eta_t \tag{2}$$

with η_t representing the prediction error of the bivariate model. A drawback is the need to set the order m, which, if set non-optimal, can result in large estimation errors.

Granger causality is then typically defined as the natural logarithm of the ratio of two prediction error variances (Ding et al., 2006), σ_ϵ^2 and σ_η^2 for the univariate and bivariate model, respectively:

$$GC_{X \to Y} = \ln \frac{\sigma_\epsilon^2}{\sigma_\eta^2} \tag{3}$$

The null hypothesis of X causing Y (or vice versa), can be tested for significance against a preset p-value, typically 5%. Thus, if $GC_{X \to Y}$ exceeds the preset threshold, assuring that σ_η^2 is significantly smaller than σ_ϵ^2, X is said to have a causal effect on Y. Similarly, the causal effect of Y on X can be determined. Note that as the effect of autocorrelation is removed, a simple correlation between X and Y does not guarantee the presence of Granger causality as co-movement does not necessarily imply causality (Aldrich, 1995).

This framework can also be extended to the multivariate case, where the effect of predictors X, Z_1, Z_2 ... Z_p (with $p+1$ the number of predictor variables) on Y can be evaluated. In order to determine the effect of X on Y in a multivariate case, the performance of a model containing all predictors is compared against that of a multivariate model from which X is excluded, as given by:

$$y_t = \sum_{i=1}^{m} a_i y_{t-i} + \sum_{j=1}^{p} (\sum_{i=1}^{m} b_{j,i} z_{j,t-i}) + \epsilon_{x,t} \tag{4}$$

$$y_t = \sum_{i=1}^{m} a_i y_{t-i} + \sum_{j=1}^{p} (\sum_{i=1}^{m} b_{j,i} z_{j,t-i}) + \sum_{i=1}^{m} c_i x_{t-i} + \eta_t \tag{5}$$

The added value of incorporating X in the set of predictors (Z_1, Z_2 ... Z_p) to improve the prediction of Y can be expressed in terms of Granger causality as:

$$GC_{X \to Y} = \ln \frac{\sigma_{\epsilon_X}^2}{\sigma_\eta^2} \tag{6}$$

2.2.2 Spectral Granger Causality

Inherent to the use of discrete time series, traditional Granger causality can only address short-term interactions, i.e. one variable at a past time-step affecting other variables in the current or future time-step. Consequently, Granger causality frameworks

https://doi.org/10.5194/bg-2019-212
Preprint. Discussion started: 14 June 2019

that are defined in the time domain, such as the newly-developed framework of Papagiannopoulou et al. (2017a), all fail to capture low-frequency processes. To assess scale-dependent processes, transforming the data into a frequency-dependent domain is crucial as it allows to differentiate between interactions active at various temporal scales. Therefore, we propose the use of CSGC, which enables to simultaneously condition for other predictors, thus factoring out co-dependency among variables, while addressing processes active at different scales.

The spectral Granger causality (SGC) is an non-parametric extension of the Granger causality theory in which timeseries are first transformed into a frequency domain, resulting in a spectral analogue of Granger causality (Geweke, 1982). A well-known example of such a transformation is the Fourier transformation, where a time series is decomposed in a space solely consisting of frequency. This allows for highlighting strong spectral features, but comes at the cost of time localisation, i.e. the ability to differentiate between processes active at different times. To prevent the loss of the time dimension, SGC adopts a wavelet transformation, which decomposes the original time series into a time–frequency space, thus allowing for both spectral (i.e. scale-dependent) evaluation and time localisation of interactions between predictors and target variable. To overcome the limitation of assigning an arbitrary order of the system given by Eq. 1 and 2, Dhamala et al. (2008) developed a non-parametric method to express spectral Granger causality based on spectral properties of the variables without the need to estimate the model order, given by:

$$SGC_{X\to Y}(f) = \ln \frac{S_{yy}(f)}{S_{yy}(f) - \left[\Gamma_{xx} - \left(\frac{\Gamma_{yx}^2}{\Gamma_{yy}}\right)\right] |H_{yx}(f)|^2} \tag{7}$$

where $S_{yy}(f)$ equals the spectral density (power spectrum) of the target variable Y at frequency f, which can be estimated from the wavelet transform. Using the variables X and Y, the error covariance matrix Γ and the spectral transfer function matrix $H(f)$ can be calculated using matrix factorisation (Wilson, 1972).

2.2.3 Conditional Spectral Granger Causality

Eq. 7 is only valid to determine the effect of a variable X on Y, without taking into account that other variables might influence both the predictor and target, consequently inducing an apparent causal relationship. To tackle this issue, conditionality between variables has to be taken into account, for which the SGC framework can be extended to conditional spectral Granger causality (CSGC). In other words, SGC can be adapted to CSGC to assess if X causes Y given that Z_1, Z_2 ... Z_p may cause Y and X, resulting in a conditioned measure of spectral causality $CSGC_{X\to Y|Z_2,Z3...Z_p}(f)$. For a multivariate problem with p+2 variables (Y, X, Z_1, Z_2 ... Z_p), the system can be written, after spectral transformation and Wilson factorisation (Wilson, 1972), as:

$$\mathbf{S}(Y, X, Z_1, Z_2 ... Z_p, f) = \mathbf{H}(f)\,\mathbf{\Sigma}\,\mathbf{H}^*(f) \tag{8}$$

$$\mathbf{U}(Y, Z_1, Z_2 ... Xp, f) = \mathbf{G}(f)\,\mathbf{\Gamma}\,\mathbf{G}^*(f) \tag{9}$$

with $\mathbf{S}$ and $\mathbf{U}$ representing the spectral matrices of the complete system and the system with the variable whose causality is tested being excluded, i.e. X in this case, respectively. Similarly, $\mathbf{H}$ and $\mathbf{G}$ are the spectral transfer function matrices, while

https://doi.org/10.5194/bg-2019-212
Preprint. Discussion started: 14 June 2019

$\sum$ and $\mathbf{\Gamma}$ equal the error covariance matrix of the full and incomplete system of variables, respectively, and where * indicates matrix adjoint.

From Eq. 8 and 9, CSGC of X on Y given Z_1, Z_2 ... Z_p can be calculated as:

$$CSGC_{X\rightarrow Y|Z_1,Z_2...Z_p}(f) = \ln \frac{\Gamma_{yy}}{|Q_{yy}(f)\Sigma_{xx}Q^*_{yy}f|} \tag{10}$$

where:

$$\mathbf{Q} = \begin{pmatrix} \tilde{G}_{YY} & 0 & \tilde{G}_{YZ_1} & ... & \tilde{G}_{YZ_p} \\ 0 & 1 & 0 & ... & 0 \\ \tilde{G}_{Z_1Y} & 0 & \tilde{G}_{Z_1Z_1} & ... & \tilde{G}_{Z_1Z_p} \\ ... & ... & ... & ... & ... \\ \tilde{G}_{Z_pY} & 0 & \tilde{G}_{Z_pZ_1} & ... & \tilde{G}_{Z_pZ_p} \end{pmatrix}^{-1} \begin{pmatrix} \tilde{H}_{YY} & \tilde{H}_{YX} & ... & ... & \tilde{H}_{YZ_p} \\ \tilde{H}_{XY} & ... & ... & ... & ... \\ ... & ... & ... & ... & ... \\ ... & ... & ... & ... & ... \\ \tilde{H}_{Z_pY} & \tilde{H}_{Z_pX} & ... & ... & \tilde{H}_{Z_pZ_p} \end{pmatrix} \tag{11}$$

In Eq. 11, $\tilde{\mathbf{H}}(f) = \mathbf{H}(f)\mathbf{P}^{-1}$ and $\tilde{\mathbf{G}} = \mathbf{G}\mathbf{P}_2^{-1}$ represent corrected transfer function matrices to separate the directional interactions (Geweke, 1982). The rotation matrices $\mathbf{P}$ are normalisation matrices needed to transform the multivariate systems in their canonical form with uncorrelated errors (Detto et al., 2013). For more information on CSGC, we refer to Dhamala et al. (2008) and Detto et al. (2012, 2013).

Using Eq. 10, spectral Granger causality of X on Y can be determined, given the influence of Z_1, Z_2 ... Z_p on both X and Y. If X is not directly affecting Y, but for example Z_1 is forcing both X and Y, the numerator in Eq. 10 will equal the denominator, thus resulting in a Granger causality measure of zero. However, if there is a direct causal influence of X on Y at a specific frequency f, $CSGC_{X\rightarrow Y|Z_1,Z_2...Z_p}(f) > 0$.

2.2.4 Significance testing of CSGC

Despite the ability of Eq. 10 to account for conditional effects between variables, it fails to determine how robust the found interactions are. Therefore, the robustness of the determined CSGC values needs to be tested against the null hypothesis that X has no causal effects on Y. In case of Granger causality in the time domain, significance of the determined statistic, e.g. GC, can be tested by a bootstrapping scheme in which the time series are randomly shuffled before determining the GC-values. By repeating this procedure n times, the distribution of GC can be determined. By selecting a p-value, typically 5%, the determined Granger causality of X on Y can be tested against the null hypothesis of no causal interaction.

However, for the spectral variant of Granger causality, a simple randomisation of the time series induces unwanted artefacts. Due to the spectral nature of the method, the power spectrum of the randomised time series must be preserved, i.e. to be equal to that of the original time series at each frequency. In other words, if the original time series are characterised by much high-frequency variation and less at lower frequencies, the time series used for significance testing need to show the same frequency-dependent variability. Therefore, surrogate time series exhibiting the same spectral power as the original time series need to be used. Here, iterative amplitude adjusted Fourier transform (IAAFT) surrogates are used in combination with Monte Carlo simulations, as CSGC is non-parametric (Detto et al., 2012), to test the determined CSGC-value against the null

https://doi.org/10.5194/bg-2019-212
Preprint. Discussion started: 14 June 2019

hypothesis of no causal interaction. Due to computational restraints, 100 runs with surrogates were run for each set of original time series (i.e. for each pixel). However, to increase robustness of the results, a p-value of 1% is chosen to compensate for the limited amount of repetitions.

2.2.5 Explained variance

CSGC as defined by Eq. 10, compares the performance of two autoregressive models in explaining variation in a target variable Y. In other words, does X, given a set of predictors Z_1, Z_2 ... Z_p, improve the estimate of Y compared to a model that only uses Z_1, Z_2 ... Z_p. In this study, we are interested in quantifying how much of variance in the target variable is actually directly explained by a predictor, and not how much did the estimation error improve upon adding X to the set of the predictors. Therefore, we deviate from the traditional formulation of Granger causality and define a new measure, the fraction (F) of variance in the target variable Y that is explained by a predictor X. Ideally, the new formulation would be:

$$F_{X\to Y} = \frac{\sigma_X^2}{\sigma_Y^2} \times 100\% \tag{12}$$

with, σ_Y^2 representing the total variance of Y and σ_X^2 the variance in Y explained by X. However, a part of the variance in Y is not explainable by any predictor, as is is forced by the autocorrelation of Y ($\sigma_{Y,auto}^2$). Therefore, in order to account for the part of variance in Y that will not be able to be explained by any predictor, Eq. 12 is adapted to:

$$F_{X\to Y} = \frac{\sigma_X^2}{\sigma_Y^2 - \sigma_{Y,auto}^2} \times 100\% \tag{13}$$

As traditional Granger causality and CSGC determine a measure of causality that is defined in a similar way, Eq. 1 can be used to determine how F can be calculated from the actual Granger causality value. Considering the univariate model given by Eq. 1, the total variance in the target variable Y can be rewritten as:

$$\sigma_Y^2 = \sigma_{Y,auto}^2 + \sigma_\epsilon^2 \tag{14}$$

with σ_ϵ^2 representing the unexplained variance or prediction error variance. Substituting Eq. 14 into Eq. 13 results in:

$$F_{X\to Y} = \frac{\sigma_X^2}{\sigma_\epsilon^2} \times 100\% \tag{15}$$

This derivation can also be extended towards the multivariate case, and even to CSGC. As Eq. 15 equals $1 - e^{-GC_{X\to Y}}$, the conditional spectral variant of the fraction of variance in Y explained by X can be calculated as:

$$F_{X\to Y|Z_1,Z_2\ldots Z_p}(f) = \frac{\Gamma_{yy} - |Q_{yy}(f)\Sigma_{xx}Q_{yy}^* f|}{\Gamma_{yy}} \times 100\% \tag{16}$$

Using Eq. 16, the impact of climate on vegetation and the feedbacks of vegetation on climate can be quantified and reported in an intuitive manner (see Sect. 3).

https://doi.org/10.5194/bg-2019-212
Preprint. Discussion started: 14 June 2019


Biogeosciences Discussions Open Access EGU

2.2.6 Determining scales of interest

As pointed up in the Sect. 1, monthly interactions between climate and vegetation have been studied by many authors (Nemani et al., 2003; Wu et al., 2015; Papagiannopoulou et al., 2017b). On the other hand, the phenological cycle or inter-annual variability of climate and vegetation are also expected to interact, yet little is known about how these interactions differ from the short-term processes. CSGC is ideal to assess these differences as it allows to simultaneously analyse interactions at different temporal scales, while no assumption has to be made about the direction of the interplay between climate and vegetation. However, CSGC determines the Granger causality at a wide range of temporal scales, starting at 2 months (twice the minimum temporal scale) and going up to 16.5 years.

In order to determine which range of temporal scales better represents monthly, seasonal and inter-annual interactions, an experiment with synthetic monthly time series was performed. First, a predictor variable ($X1$) is constructed with imposed variability at the scales of interest (e.g. monthly, seasonal and inter-annual). Monthly variability is assumed to be random from month to month, while seasonality is defined as consecutive three-block periods of constant value. Inter-annual variation is defined as blocks of one year with a fixed value. The predictor $X1$ is constructed by randomly generating these three variabilities and adding them. Finally, a linear trend is added to $X1$ to be able to retrieve the maximum scale at which inter-annual variability can be observed. Next, a target variable ($Y1$) is constructed with a known causal relation to the predictor $X1$ by multiplying $X1$ with a random factor and then shifting $Y1$ in time so that $Y1$ lags $X1$ by one month. Using these two synthetic time series, SGC is used to determine the Granger causality of $X1$ on $Y1$. Note that SGC is used instead of CSGC as the scales at which the targeted interactions can be observed are identical for a bivariate and multivariate case.

In order to identify the scales that are most sensitive to monthly, seasonal and inter-annual interactions, a new predictor variable $X2$ is constructed as an identical copy of $X1$, except for one specific variability. For example, if the range of scales that capture monthly interactions is determined, $X2$ will be equal to $X1$, but with perturbed monthly variability. Next, a new target variable $Y2$ is constructed by multiplying $X2$ with a new random factor and again guaranteeing that $Y2$ lags $X2$ by one month. Then, SGC is used to determine if $X1$ Granger causes $Y2$, which will show a decrease in Granger causality at scales that capture the perturbed interaction compared to the Granger causality of $X1$ on $Y1$. Consequently, by repeating this procedure for all the interactions that are to be assessed (i.e. monthly, seasonal and inter-annual), comparison of the two Granger causalities allows to record the range of scales that capture these interactions. To increase robustness, this procedure is repeated 100,000 times, resulting in a clear delineation of scales representing monthly (0–0.32 years), seasonal (0.32–1.54 years) and inter-annual (1.54–9 years) interactions. Decadal patterns of trends cannot be investigated here due to length of the observational record (see Sect. 2.1), but are used in the determination of the ranges to fix the upper limit for inter-annual interactions. See Fig. 1 for an illustration of the resulting scales, which are considered to be time- and space-invariant. Results will be presented as mean patterns for each scale using the determined ranges. Selecting the maximum explained variance within each range, unwillingly results in the taking the CSGC at the highest scale of each interval, as the CSGC increases with the scale (for more information, see Sect. 3.1).

https://doi.org/10.5194/bg-2019-212
Preprint. Discussion started: 14 June 2019

3 Results and discussion

3.1 Climate impact on vegetation in observations

Fig. 2 illustrates the Granger causality of precipitation, air temperature and net radiation on LAI dynamics, based on observations (Fig. 2a, 2c, 2e), globally and latitudinally. Results are shown separately for monthly (Fig. 2a), seasonal (Fig. 2c) and inter-annual (Fig. 2e) time-scales using a tri-variate colormap according to the fraction explained by each climatic driver (see Sect. 2.2.5). Dotted pixels highlight significance of the strongest climate impact on vegetation at a 1%-significance level. At monthly scales, overall spatial patterns in the observation-based results (Fig. 2a) are in agreement with previous studies, showing the dominance of precipitation in arid and semi-arid regions, while radiation and temperature dominate in northern latitudes and rainforests (Nemani et al., 2003; de Jong et al., 2013; Seddon et al., 2016; Papagiannopoulou et al., 2017b). Strong radiation effects on vegetation can be observed over northern latitudes due to severe limitations in incoming radiation during winter months. Recently, Papagiannopoulou et al. (2017b) reported, based on a non-linear Granger causality framework, that 61% of the vegetated land surface is primarily driven by water availability at monthly time scales, while temperature and radiation are the primary factors in only 23% and 15% of the vegetated surface (respectively). These results contrasted strongly with earlier studies, that pointed to a less dominant role of water availability for global ecosystems (Nemani et al., 2003; Wu et al., 2015). Here, our monthly-scale results also highlight a more moderate role of precipitation, which dominates (i.e is highest) in 41% of the vegetated land, with radiation being the primary control factor in 41% as well. However, when the analysis targets vegetation anomalies by detrending linearly and subtracting the average seasonal cycle (as was done in Papagiannopoulou et al. (2017a, b)), the results show precipitation and air temperature gaining importance over net radiation as they are the dominant driver over 45%, 21% and 33%, respectively, as indicated in Supplementary Fig. A1. Using anomalies results to a slight increase of the importance of precipitation, but Papagiannopoulou et al. (2017b) also accounted directly for the effect of (root-depth) soil moisture as a driver of water availability, consequently increasing the dominance of precipitation. Finally, the lower water limitation in the northern latitudes (Fig. 2a) relates to the fact that Papagiannopoulou et al. (2017b) considered also snow water equivalent as a water availability driver. Evenmore, the framework used by Papagiannopoulou et al. (2017b) incoporates a battery of remotely-sensed products, which can widely diverge and consequently lead to discrepancies in the results. This also reconciles the results in Papagiannopoulou et al. (2017b) with previous studies such as Nemani et al. (2003), Wu et al. (2015), and Seddon et al. (2016) that focused on other temporal scales or used different variables to assess water availability.

As mentioned before, a key feature of CSGC is that it also enables the assessment of interactions at longer temporal scales, such as seasonally (Fig. 2c) and inter-annually (Fig. 2e). Radiation is found to dominate the seasonal phenology over 51% of the global vegetated land. The strong radiation control over northern latitudes is attributed to the amplitude of the solar cycle, which ultimately inhibits vegetation growth during wintertime. In this analysis, net radiation instead of incoming radiation has been used, in order to be consistent with the investigation of vegetation–climate feedbacks in Sect. 3.3; however, using incoming radiation as driver instead, leads to a similar 50% dominance (see Fig. B1). Compared to monthly scales, the importance of precipitation as a driver of vegetation decreases in regions such as the Mediterranean region and western South America that

https://doi.org/10.5194/bg-2019-212
Preprint. Discussion started: 14 June 2019

still show the dominant role of radiation forcing vegetation phenology, while hotspots of temperature-driven phenology are found over the Sahel region and south of the Congo rainforest. Furthermore, the results for seasonal scales in Amazonia tend to agree with the findings of Saleska et al. (2007), Phillips et al. (2009), Hilker et al. (2014), and Saleska et al. (2016), showing a dominance of water availability in the southeastern side, while radiation is more limiting in the northwest. Overall, precipitation primarily controls ecosystem phenology in (semi-)arid regions, adding up to 30% of the vegetated land (Fig. 2c).

Finally, at inter-annual scales, global ecosystems tend to be more water limited: 46% of the vegetated land surface is primarily dominated by precipitation (Fig. 2e). Although patterns appear highly heterogeneous, not only arid and semiarid regions show a dominant control by precipitation, but also substantial parts of continental Eurasia and North America, albeit the results for most of these regions are not statistically significant. This inter-annual dependency of ecosystem dynamics on water availability may arise due to the large inter-annual variability of precipitation – compared to e.g, radiation – and has already been documented in relation to the impact of precipitation of global carbon budgets (Poulter et al., 2014) and terrestrial evaporation (Miralles et al., 2014). Air temperature thrives scattered over the high northern latitudes, dominating in 28% of vegetated land, while radiation is typically less crucial than the other two drivers at inter-annual scales, likely due to its lower inter-annual variability as mentioned above. Nonetheless, the overall control of climate on vegetation is higher at inter-annual scales than at shorter time scales, as can be observed in the latitudinal profiles, which show the total causality in absolute terms (Fig. 2). This is partly a consequence of the time-frequency decomposition of CSGC, which generally results in higher values of explained variance at longer timescales due to the increased time frame over which a predictor variable is assessed, thus increasing the chance of incorporating memory effects. However, during the significance test against the null hypothesis of exhibiting no causal effect, the calculated threshold for significance also increases with the temporal scales, consequently ensuring that regions exhibiting significant responses can be compared over different timescales. The dominant role of water availability at inter-annual scales, agrees with the results of Green et al. (2019) and Humphrey et al. (2018), yet it does not necessarily contradict the results by Jung et al. (2017); the latter reports a dominant role of temperature at the global scale, yet shows a clear dominance of water availability at regional scales, that is compensated when upscaling to global means.

3.2 Climate impact on vegetation in models

Results of the observations are next used to benchmark CMIP5 ESM performance in representing the control of climate on vegetation (Fig. 2b, 2d, 2f). Dotted pixels indicate that at least three models find the same climate driver to be the significant primary control of vegetation at a 1%-significance level. At monthly scales, comparison of Fig. 2a and 2b shows that the impact of air temperature on ecosystems is strongly overestimated by ESMs, with 17% and 26% of vegetated land being primarily dominated by temperature for observations and ESMs, respectively. This coincides with a lower effect of net radiation in central Eurasia and, more importantly, in the Amazon and Congo rainforests. These contrasting results with observations might hint towards problems in ESMs with respect to representing the behaviour of the tropics, but may also relate to the difficulties to retrieve LAI from satellites in dense tropical forests (Hilker et al., 2015). Nevertheless, ESMs agree on the general patterns that highlight the strong radiation effects in northern latitudes (albeit less extended), and the water availability as main driver in arid and semiarid regions.

https://doi.org/10.5194/bg-2019-212
Preprint. Discussion started: 14 June 2019

Seasonally, a larger control of climate on vegetation phenology is also noticeable over the equator for ESMs (Fig. 2d). The dominant control of radiation on vegetation phenology over northern latitudes is similar for all models (inter-model agreement and significance represented by the black dotting), and agrees with the observational results (see Fig. 2c). Radiation is the primary driver of the seasonal LAI variation in 40% of the vegetated land in models (compared to 51% for the observations). The role of precipitation and air temperature as a driver of the phenological cycle gains in importance in ESMs, at the cost of radiation, with 34% and 24% of seasonal LAI variation being dominated by precipitation and air temperature variability, respectively, versus the 30% and 17% in observations, respectively. Despite the overall similarities in the patterns of dominant drivers, regional differences between observations and models are still observed. Models point towards a water-limited phenological cycle in the Sahel, while observations hint also towards a dominant role of temperature. Furthermore, whereas observations clearly highlight a south-to-north water-to-energy-limited gradient in Amazonia, models tend to disagree and point towards temperature as a key driver over most the Amazonian rainforest at seasonal scales. These differences might indicate difficulties to model climate–vegetation interactions across the basin, yet they may again be influenced by the difficulties to retrieve LAI from satellites over dense canopies.

Similar to observations, the climate impact on LAI increases with longer temporal scales in ESMs. More remarkable than in the observations, is the strong water limitation across the globe at inter-annual scales, which is not restricted to the typical arid and semi-arid regions (Fig. 2f). Water availability at inter-annual scales is dominant for vegetation over 52% of land versus the 46% found in observations (Fig. 2e). However, this divergence between observations and models is also influenced by the shorter record of satellite data, which, as mentioned above, is expected to affect the results at longer (e.g., inter-annual) temporal scales.

3.3 Vegetation feedback on climate in observations and models

Analogous to the effect of climate on vegetation, vegetation can alter local (and remote) climate conditions via biophysical and biochemical feedbacks. These feedbacks arise from the effect of vegetation structure and physiological activity on the surface radiation budget, available energy partitioning into latent and sensible heat fluxes, aerodynamic conductance of the ecosystem, atmospheric chemical composition, and indirect processes affecting incoming radiation, atmospheric humidity and temperature (McPherson, 2007; Bonan, 2008). The representation of these feedbacks in ESMs remains in need for improvement to accurately predict future climate (de Noblet-Ducoudré et al., 2012; Zhang et al., 2016). Here, we unravel these feedbacks of LAI on different climate variables based on observations (Fig. 3a, 3c, and 3e) and ESM data (Fig. 3b, 3d, and 3f), and at different temporal scales, from monthly (Fig. 3a and 3b), to seasonal (Fig. 3c and 3d) and inter-annual (Fig. 3e and 3f). Dotted pixels indicate significance at the 1%-level of the strongest feedback (for observations, e.g. Fig. 3a, 3c, and 3e), or three models agreeing on the significance of the strongest feedbacks (Fig. 3b, 3d, and 3f). To aid comparison to the strength of climate impacts on vegetation – measured in relative or absolute percentage of caused variance (see Sect. 2.2.5) – an identical tri-variate colormap to that in Fig. 2 is used.

Observed LAI feedbacks over the mid and high northern latitudes mainly reflect on the direct impact on surface net radiation at monthly time scales (Fig. 3a). As vegetation lowers the surface albedo in boreal regions, it allows for more energy storage

https://doi.org/10.5194/bg-2019-212
Preprint. Discussion started: 14 June 2019

and less reflection back into the atmosphere; this increases net radiation and may lead to a net warming effect (e.g. Bonan, 2008; Forzieri et al., 2017). By repeating the analysis using only incoming (shortwave and longwave) radiation, instead of surface net radiation, the results indicate that the influence of LAI on cloud formation is limited, at least considering the local scales revealed by the causal framework (see Fig. C1). Monthly feedbacks of vegetation on precipitation and air temperature are spatially heterogeneous and weaker. Seasonally, two distinct areas of significant effect (see dotted pixels) of LAI on precipitation can be distinguished, namely southern Amazonia and the Congo rainforest. Patterns in Amazonia suggest a more dominant effect of vegetation on radiation in the north, while precipitation feedbacks dominate in the south. We note that the method does not differentiate whether higher or lower values of LAI cause more or less rainfall, only that a causal effect of LAI on rainfall exists. The south-to-north patterns in the Amazon agree with the larger dependency on precipitation recycling in the South (Dirmeyer et al., 2009; Zemp et al., 2014). Tropical forests are known to regulate local (and global) precipitation as their large use of water increases atmospheric humidity and results in cloud formation (Malhi et al., 2008). This also directly affects the incoming short- and long-wave radiation. However, we restate that the method only focuses on the effects of LAI on its immediate climatic environment, not in neighbouring or remote locations. Seasonal feedbacks are more clear for radiation and air temperature, although their statistical significance is lower (Fig. 3c); however, these results do indicate to an effect of LAI on the seasonal cycle of the ecosystem energy budget, albeit less significant as for monthly interactions.

Finally, the observation-based results suggest that feedbacks cannot be clearly disentangled at inter-annual scales using the CSGC, as shown by the incoherent spatial patterns in Fig. 3e. This may occur due to the long integration time and the somehow limited observational record. Overall, and as expected, comparisons between Fig. 2 and 3 reveal that the impact of climate on vegetation consistently exceeds the strength of the vegetation feedback on climate. This can be partly attributed to the fact that only local interactions are considered here: while vegetation reacts to its most immediate environment, vegetation can lead to remote effects on climate that are not addressed in our analyses (Dirmeyer et al., 2009; Guillod et al., 2015). Nevertheless, these results show the importance of LAI variability in explaining the variance in local climate at intra-annual scales – mainly through impacts on the net radiation induced by albedo changes – and the potential of the CSGC framework to disentangle the bi-directional interaction between vegetation and climate.

ESMs capture correctly the LAI effects on net radiation throughout most of the Northern Hemisphere. While models only agree with each other in the influence of LAI on net radiation in very high northern latitudes (see dotted pixels), the mean ensemble patterns agree well with observational results, for both monthly and seasonal timescales. Interestingly, while observations show significant impacts of LAI on precipitation in the edges of the tropical forests, these effects are not reproduced by ESMs, which tend to show a larger influence of LAI on temperature in the tropics. This may suggest a lower dependency of tropical forests on rainfall recycling (Malhi et al., 2008; Hilker et al., 2014; Zemp et al., 2017) and/or an overall wet bias in the ESMs (Mueller and Seneviratne, 2014); the latter is however not supported by the results in Fig. 2 that indicate an overall overestimation of water limitations in models. Nonetheless, these feedbacks on temperature and precipitation are overall weak – both in observations and models – as indicated by the absolute magnitudes shown in the latitudinal profiles.

https://doi.org/10.5194/bg-2019-212
Preprint. Discussion started: 14 June 2019

3.4 Biome-specific interactions

Finally, to better visualise the multi-scale vegetation–climate interactions in observations and models, results are presented averaged per biome type. Fig. 4 shows the biome-averaged absolute observed and modelled climate control on LAI dynamics, while Fig. 5 presents the vegetation feedbacks on climate. Both boreal and tropical forests are found to be mostly energy-driven, in agreement with previous studies (Nemani et al., 2003; Seddon et al., 2016; Papagiannopoulou et al., 2017b). ESMs tend to agree with the observations on the magnitude of the response of ecosystems to radiation at all temporal scales, with the exception of the over-sensitivity of evergreen broadleaf forests (EBF) at monthly scales and for most models. In regards to the influence of air temperature, even though ESMs agree with each other, strong differences with observations can be observed at seasonal timescales for most forest biomes; this is remarkable for broadleaf forests, both evergreen and deciduous (EBF and DBF), which show a model overestimation of the control of temperature control on LAI dynamics. Interestingly, models also overestimate the sensitivity of broadleaf forests (EBF and DBF) to precipitation at seasonal and inter-annual timescales. Observation results show limited water stress in tropical and mid-latitude forests, arguably due to the deep rooting system and mild climate. However, this apparent model over-dependency of broadleaf forests on climate may also emerge from the under-sensitivity of the observational results due to the saturation of the greenness signal received by satellites in dense canopies. Models unambiguously overestimate the importance of water availability for LAI in most biome types, and for all three timescales, with the exception of open shrublands (OS) and grasslands (G). This appears in contrast with the results of Green et al. (2017). As expected, savannas are found to be mainly driven by precipitation across all timescales both in observations and models, although models strongly disagree among each other, as reflected by the large error bars in Fig. 4.

On the other hand, short-term feedbacks of LAI on climate seem to be well represented in ESMs, as small differences can be seen when compared to the observational results in Fig. 5. Deciduous (DNF) and evergreen (ENF) needleleaf forests exhibit the strongest feedback net radiation (and temperature) at all temporal scales; once again this appears related to albedo changes and not impacts on, e.g., cloud formation (see Fig. C1). Nonetheless, the effect of needleleaf forests on the radiation budget tends to be overestimated by most CMIP5 models, especially at monthly and seasonal time scales. ESMs also overestimate the influence of ecosystem phenology on net radiation in mixed forests (MF), open shrublands (OS), and woody savannas (WS); yet, large inter-model disagreements exist on the seasonal influence of LAI on net radiation for almost all biomes, as illustrated by the large error bars Fig. 5). The strength of the effect of LAI on precipitation is overall lower than its impact on net radiation and air temperature, partly due to the less localised influence and the non-consideration of downwind influences in this analysis. Contrary to the results of Green et al. (2017), no particular influence of LAI on precipitation can be observed for semi-arid regions, although these regions have been found to be able to offset decreases in precipitation when considering non-local mechanisms (Miralles et al., 2016).

4 Conclusion

Here, bi-directional interactions between climate and vegetation in global remotely-sensed observations were analysed at different temporal scales using conditional spectral Granger causality (CSGC) with the aim to benchmark the representation of

https://doi.org/10.5194/bg-2019-212
Preprint. Discussion started: 14 June 2019

these interactions in ESMs. Three main climate variables are considered, namely air temperature, net radiation and precipitation, while LAI is used as a proxy for vegetation state. While CSGC is not designed to cope with non-linear interactions, it has the advantage of being able to assess both the climate impact on vegetation and the vegetation feedback on climate, while differentiating simultaneously between different temporal scales. Our findings for monthly interactions agree with those of earlier studies (Nemani et al., 2003; Wu et al., 2015; Papagiannopoulou et al., 2017b), with (semi-)arid regions showing a primary control by water-availability, while the tropics and high northern latitudes being primarily energy-limited. Fig. 6 gives an overview of the overall global interactions between climate and biosphere. Averaged over continental vegetated land, radiation is found to dominate vegetation dynamics at seasonal scale, but models seem consistently incapable of reproducing the strength of this dependency. At longer timescales, precipitation control gains in importance, but models tend to overestimate this inter-annual control of water availability. On the other hand, vegetation feedbacks are found to be most widespread for net radiation over all timescales, mainly due to the strong interplay between radiation and vegetation at northern latitudes. As shown by the summary in Fig. 6, the range of feedbacks as estimated from the ESM output includes the feedbacks from the observations, except for feedbacks on precipitation, which are often underestimated. Finally, interactions, in both ways, were found to increase with increasing timescales, and feedbacks of vegetation on climate explain a lower percentage of variance, as expected, than the climate impact on vegetation.

Despite the clear advantages over traditional statistical analysis, the application of CSGC is subject to a series of assumptions. Firstly, CSGC can condition for other variables to exclude effects due to co-dependency, but this implies that the variable has to be considered. Here, we limited the potential drivers of vegetation to air temperature, net radiation and precipitation, but vegetation is also affected by other factors such as nutrient availability, atmospheric carbon dioxide concentrations etc. Secondly, only local interactions are considered, meaning that interactions are assumed to occur within a pixel. This assumption might be valid for the impact of climate on vegetation, but is certainly an oversimplification regarding the vegetation feedbacks on climate which are rarely of local nature, especially when it refers to cloudiness and rainfall. Finally, errors in the observations due to difficulties in retrieving LAI over dense canopies, such as tropical forests, may falsely point towards process misrepresentations in ESMs, which overall show a good agreement with the observational results in our analyses.

https://doi.org/10.5194/bg-2019-212
Preprint. Discussion started: 14 June 2019

Biogeosciences Discussions
Open Access
EGU

Appendix A: Climate impact on vegetation in anomalies of observations

Appendix B: Climate impact on vegetation in observations using incoming radiation instead of net radiation

Appendix C: Vegetation feedback on climate in observations using incoming radiation instead of net radiation

https://doi.org/10.5194/bg-2019-212
Preprint. Discussion started: 14 June 2019

Author contributions. D. G. Miralles and J. Claessen conceived the study and led the writing. J. Claessen conducted the analysis. A. Molini and M. Detto contributed to the implementation of the method. All co-authors contributed to the design of the experiments, interpretation of results and editing of the manuscript.

Competing interests. The authors declare that they have no conflict of interest.

Acknowledgements. This work is funded by the Belgian Science Policy Office (BELSPO) in the framework of the STEREO III programme, projects SAT-EX (SR/00/306) and SAT-EX Wave (SR/02/367). We acknowledge the World Climate Research Programme's Working Group on Coupled Modelling, which is responsible for CMIP. We also thank the climate modelling groups for their effort in producing and making available of their model output.

https://doi.org/10.5194/bg-2019-212
Preprint. Discussion started: 14 June 2019

References

Aldrich, J.: Correlations genuine and spurious in Pearson and Yule, Statistical science, pp. 364–376, 1995.

Alessandri, A., Catalano, F., De Felice, M., Van Den Hurk, B., Reyes, F. D., Boussetta, S., Balsamo, G., and Miller, P. A.: Multi-scale enhancement of climate prediction over land by increasing the model sensitivity to vegetation variability in EC-Earth, Climate Dynamics, 49, 1215–1237, 2017.

Bentsen, M., Bethke, I., Debernard, J., Iversen, T., Kirkevåg, A., Seland, Ø., Drange, H., Roelandt, C., Seierstad, I., Hoose, C., et al.: The Norwegian earth system model, NorESM1-M — Part 1: Description and basic evaluation of the physical climate, Geoscientific Model Development, 6, 687–720, 2013.

Bonan, G. B.: Forests and climate change: forcings, feedbacks, and the climate benefits of forests, Science, 320, 1444–1449, 2008.

Collins, W., Bellouin, N., Doutriaux-Boucher, M., Gedney, N., Halloran, P., Hinton, T., Hughes, J., Jones, C., Joshi, M., Liddicoat, S., et al.: Development and evaluation of an Earth-System model–HadGEM2, Geoscientific Model Development, 4, 1051–1075, 2011.

de Jong, R., Schaepman, M. E., Furrer, R., De Bruin, S., and Verburg, P. H.: Spatial relationship between climatologies and changes in global vegetation activity, Global Change Biology, 19, 1953–1964, 2013.

De Keersmaecker, W., Lhermitte, S., Tits, L., Honnay, O., Somers, B., and Coppin, P.: A model quantifying global vegetation resistance and resilience to short-term climate anomalies and their relationship with vegetation cover, Global Ecology and Biogeography, 24, 539–548, 2015.

de Noblet-Ducoudré, N., Boisier, J.-P., Pitman, A., Bonan, G., Brovkin, V., Cruz, F., Delire, C., Gayler, V., Van den Hurk, B., Lawrence, P., et al.: Determining robust impacts of land-use-induced land cover changes on surface climate over North America and Eurasia: results from the first set of LUCID experiments, Journal of Climate, 25, 3261–3281, 2012.

Detto, M., Molini, A., Katul, G., Stoy, P., Palmroth, S., and Baldocchi, D.: Causality and persistence in ecological systems: a nonparametric spectral Granger causality approach, The American Naturalist, 179, 524–535, 2012.

Detto, M., Bohrer, G., Nietz, J., Maurer, K., Vogel, C., Gough, C., and Curtis, P.: Multivariate conditional Granger causality analysis for lagged response of soil respiration in a temperate forest, Entropy, 15, 4266–4284, 2013.

Dhamala, M., Rangarajan, G., and Ding, M.: Estimating Granger causality from Fourier and wavelet transforms of time series data, Physical Review Letters, 100, 018 701, 2008.

Ding, M., Chen, Y., and Bressler, S. L.: Granger causality: basic theory and application to neuroscience, Handbook of time series analysis: recent theoretical developments and applications, pp. 437–460, 2006.

Dirmeyer, P. A., Brubaker, K. L., and DelSole, T.: Import and export of atmospheric water vapor between nations, Journal of hydrology, 365, 11–22, 2009.

Dufresne, J.-L., Foujols, M.-A., Denvil, S., Caubel, A., Marti, O., Aumont, O., Balkanski, Y., Bekki, S., Bellenger, H., Benshila, R., et al.: Climate change projections using the IPSL-CM5 Earth System Model: from CMIP3 to CMIP5, Climate Dynamics, 40, 2123–2165, 2013.

Forkel, M., Carvalhais, N., Schaphoff, S., v. Bloh, W., Migliavacca, M., Thurner, M., and Thonicke, K.: Identifying environmental controls on vegetation greenness phenology through model–data integration, Biogeosciences, 11, 7025–7050, https://doi.org/10.5194/bg-11-7025-2014, https://www.biogeosciences.net/11/7025/2014/, 2014.

Forzieri, G., Alkama, R., Miralles, D. G., and Cescatti, A.: Satellites reveal contrasting responses of regional climate to the widespread greening of Earth, Science, 356, 1180–1184, 2017.

https://doi.org/10.5194/bg-2019-212
Preprint. Discussion started: 14 June 2019

Forzieri, G., Duveiller, G., Georgievski, G., Li, W., Robertson, E., Kautz, M., Lawrence, P., Garcia San Martin, L., Anthoni, P., Ciais, P., et al.: Evaluating the Interplay Between Biophysical Processes and Leaf Area Changes in Land Surface Models, Journal of Advances in Modeling Earth Systems, 2018.

Gent, P. R., Danabasoglu, G., Donner, L. J., Holland, M. M., Hunke, E. C., Jayne, S. R., Lawrence, D. M., Neale, R. B., Rasch, P. J., Vertenstein, M., et al.: The community climate system model version 4, Journal of Climate, 24, 4973–4991, 2011.

Geweke, J.: Measurement of linear dependence and feedback between multiple time series, Journal of the American Statistical Association, 77, 304–313, 1982.

Granger, C. W. J.: Investigating causal relations by econometric models and cross-spectral methods, Econometrica: Journal of the Econometric Society, pp. 424–438, 1969.

Green, J. K., Konings, A. G., Alemohammad, S. H., Berry, J., Entekhabi, D., Kolassa, J., Lee, J.-E., and Gentine, P.: Regionally strong feedbacks between the atmosphere and terrestrial biosphere, Nature Geoscience, 10, 410, 2017.

Green, J. K., Seneviratne, S. I., Berg, A. M., Findell, K. L., Hagemann, S., Lawrence, D. M., and Gentine, P.: Large influence of soil moisture on long-term terrestrial carbon uptake, Nature, 565, 476, 2019.

Guillod, B. P., Orlowsky, B., Miralles, D. G., Teuling, A. J., and Seneviratne, S. I.: Reconciling spatial and temporal soil moisture effects on afternoon rainfall, Nature Communications, 6, 6443, 2015.

Hilker, T., Lyapustin, A. I., Tucker, C. J., Hall, F. G., Myneni, R. B., Wang, Y., Bi, J., de Moura, Y. M., and Sellers, P. J.: Vegetation dynamics and rainfall sensitivity of the Amazon, Proceedings of the National Academy of Sciences, 111, 16 041–16 046, 2014.

Hilker, T., Lyapustin, A. I., Hall, F. G., Myneni, R., Knyazikhin, Y., Wang, Y., Tucker, C. J., and Sellers, P. J.: On the measurability of change in Amazon vegetation from MODIS, Remote Sensing of Environment, 166, 233–242, 2015.

Humphrey, V., Zscheischler, J., Ciais, P., Gudmundsson, L., Sitch, S., and Seneviratne, S. I.: Sensitivity of atmospheric CO2 growth rate to observed changes in terrestrial water storage, Nature, 560, 628, 2018.

Jung, M., Reichstein, M., Schwalm, C. R., Huntingford, C., Sitch, S., Ahlström, A., Arneth, A., Camps-Valls, G., Ciais, P., Friedlingstein, P., et al.: Compensatory water effects link yearly global land CO2 sink changes to temperature, Nature, 541, 516, 2017.

Kottek, M., Grieser, J., Beck, C., Rudolf, B., and Rubel, F.: World map of the Köppen-Geiger climate classification updated, Meteorologische Zeitschrift, 15, 259–263, 2006.

Le Quéré, C., Andrew, R. M., Friedlingstein, P., Sitch, S., Pongratz, J., Manning, A. C., Korsbakken, J. I., Peters, G. P., Canadell, J. G., Jackson, R. B., et al.: Global carbon budget 2017, Earth System Science Data, 10, 405, 2018.

Loveland, T. R. and Belward, A.: The IGBP-DIS global 1km land cover data set, DISCover: first results, International Journal of Remote Sensing, 18, 3289–3295, 1997.

Malhi, Y., Roberts, J. T., Betts, R. A., Killeen, T. J., Li, W., and Nobre, C. A.: Climate change, deforestation, and the fate of the Amazon, Science, 319, 169–172, 2008.

McPherson, R. A.: A review of vegetation—atmosphere interactions and their influences on mesoscale phenomena, Progress in Physical Geography, 31, 261–285, 2007.

Miralles, D. G., Van Den Berg, M. J., Gash, J. H., Parinussa, R. M., De Jeu, R. A., Beck, H. E., Holmes, T. R., Jiménez, C., Verhoest, N. E., Dorigo, W. A., et al.: El Niño–La Niña cycle and recent trends in continental evaporation, Nature Climate Change, 4, 122, 2014.

Miralles, D. G., Nieto, R., McDowell, N. G., Dorigo, W. A., Verhoest, N. E., Liu, Y. Y., Teuling, A. J., Dolman, A. J., Good, S. P., and Gimeno, L.: Contribution of water-limited ecoregions to their own supply of rainfall, Environmental Research Letters, 11, 124 007, 2016.

https://doi.org/10.5194/bg-2019-212
Preprint. Discussion started: 14 June 2019

Mueller, B. and Seneviratne, S. I.: Systematic land climate and evapotranspiration biases in CMIP5 simulations, Geophysical Research Letters, 41, 128–134, 2014.

Murray-Tortarolo, G., Anav, A., Friedlingstein, P., Sitch, S., Piao, S., Zhu, Z., Poulter, B., Zaehle, S., Ahlström, A., Lomas, M., Levis, S., Viovy, N., and Zeng, N.: Evaluation of Land Surface Models in Reproducing Satellite-Derived LAI over the High-Latitude Northern Hemisphere. Part I: Uncoupled DGVMs, Remote Sensing, 5, 4819–4838, http://www.mdpi.com/2072-4292/5/10/4819, 2013.

Nemani, R. R., Keeling, C. D., Hashimoto, H., Jolly, W. M., Piper, S. C., Tucker, C. J., Myneni, R. B., and Running, S. W.: Climate-driven increases in global terrestrial net primary production from 1982 to 1999, Science, 300, 1560–1563, 2003.

Pachauri, R. K., Allen, M. R., Barros, V. R., Broome, J., Cramer, W., Christ, R., Church, J. A., Clarke, L., Dahe, Q., Dasgupta, P., et al.: Climate change 2014: synthesis report. Contribution of Working Groups I, II and III to the fifth assessment report of the Intergovernmental Panel on Climate Change, IPCC, 2014.

Papagiannopoulou, C., Miralles, D. G., Decubber, S., Demuzere, M., Verhoest, N. E. C., Dorigo, W. A., and Waegeman, W.: A non-linear Granger-causality framework to investigate climate–vegetation dynamics, Geoscientific Model Development, 10, 1945, 2017a.

Papagiannopoulou, C., Miralles, D. G., Dorigo, W. A., Verhoest, N. E. C., Depoorter, M., and Waegeman, W.: Vegetation anomalies caused by antecedent precipitation in most of the world, Environmental Research Letters, 12, 074 016, 2017b.

Pearson, R. G., Phillips, S. J., Loranty, M. M., Beck, P. S., Damoulas, T., Knight, S. J., and Goetz, S. J.: Shifts in Arctic vegetation and associated feedbacks under climate change, Nature Climate Change, 3, 673, 2013.

Phillips, O. L., Aragão, L. E., Lewis, S. L., Fisher, J. B., Lloyd, J., López-González, G., Malhi, Y., Monteagudo, A., Peacock, J., Quesada, C. A., et al.: Drought sensitivity of the Amazon rainforest, Science, 323, 1344–1347, 2009.

Piao, S., Sitch, S., Ciais, P., Friedlingstein, P., Peylin, P., Wang, X., Ahlström, A., Anav, A., Canadell, J. G., Cong, N., et al.: Evaluation of terrestrial carbon cycle models for their response to climate variability and to CO2 trends, Global Change Biology, 19, 2117–2132, 2013.

Poulter, B., Frank, D., Ciais, P., Myneni, R. B., Andela, N., Bi, J., Broquet, G., Canadell, J. G., Chevallier, F., Liu, Y. Y., et al.: Contribution of semi-arid ecosystems to interannual variability of the global carbon cycle, Nature, 509, 600, 2014.

Randerson, J. T., Hoffman, F. M., Thornton, P. E., Mahowald, N. M., Lindsay, K., LEE, Y.-H., Nevison, C. D., Doney, S. C., Bonan, G., Stöckli, R., et al.: Systematic assessment of terrestrial biogeochemistry in coupled climate–carbon models, Global Change Biology, 15, 2462–2484, 2009.

Saleska, S. R., Didan, K., Huete, A. R., and Da Rocha, H. R.: Amazon forests green-up during 2005 drought, Science, 318, 612–612, 2007.

Saleska, S. R., Wu, J., Guan, K., Araujo, A. C., Huete, A., Nobre, A. D., and Restrepo-Coupe, N.: Dry-season greening of Amazon forests, Nature, 531, E4, 2016.

Schimel, D., Stephens, B. B., and Fisher, J. B.: Effect of increasing CO2 on the terrestrial carbon cycle, Proceedings of the National Academy of Sciences, 112, 436–441, 2015.

Seddon, A. W., Macias-Fauria, M., Long, P. R., Benz, D., and Willis, K. J.: Sensitivity of global terrestrial ecosystems to climate variability, Nature, 531, 229, 2016.

Stocker, B. D., Zscheischler, J., Keenan, T. F., Prentice, I. C., Seneviratne, S. I., and Peñuelas, J.: Drought impacts on terrestrial primary production underestimated by satellite monitoring, Nature Geoscience, p. 1, 2019.

Taylor, K. E., Stouffer, R. J., and Meehl, G. A.: An overview of CMIP5 and the experiment design, Bulletin of the American Meteorological Society, 93, 485–498, 2012.

Viovy, N.: CRUNCEP Version 7 - Atmospheric Forcing Data for the Community Land Model, http://rda.ucar.edu/datasets/ds314.3/, accessed Februari 2018, 2018.

https://doi.org/10.5194/bg-2019-212
Preprint. Discussion started: 14 June 2019

Weiss, M., van den Hurk, B., Haarsma, R., and Hazeleger, W.: Impact of vegetation variability on potential predictability and skill of EC-Earth simulations, Climate Dynamics, 39, 2733–2746, 2012.

Wilson, G. T.: The factorization of matricial spectral densities, SIAM Journal on Applied Mathematics, 23, 420–426, 1972.

Wu, D., Zhao, X., Liang, S., Zhou, T., Huang, K., Tang, B., and Zhao, W.: Time-lag effects of global vegetation responses to climate change, Global Change Biology, 21, 3520–3531, 2015.

Zemp, D., Schleussner, C.-F., Barbosa, H., Van der Ent, R., Donges, J. F., Heinke, J., Sampaio, G., and Rammig, A.: On the importance of cascading moisture recycling in South America, Atmospheric Chemistry and Physics, 14, 13 337–13 359, 2014.

Zemp, D. C., Schleussner, C.-F., Barbosa, H. M., Hirota, M., Montade, V., Sampaio, G., Staal, A., Wang-Erlandsson, L., and Rammig, A.: Self-amplified Amazon forest loss due to vegetation-atmosphere feedbacks, Nature Communications, 8, 14 681, 2017.

Zeng, Z., Piao, S., Li, L. Z., Zhou, L., Ciais, P., Wang, T., Li, Y., Lian, X., Wood, E. F., Friedlingstein, P., et al.: Climate mitigation from vegetation biophysical feedbacks during the past three decades, Nature Climate Change, 7, 432, 2017.

Zhang, Y., Peña-Arancibia, J. L., McVicar, T. R., Chiew, F. H., Vaze, J., Liu, C., Lu, X., Zheng, H., Wang, Y., Liu, Y. Y., et al.: Multi-decadal trends in global terrestrial evapotranspiration and its components, Scientific Reports, 6, 19 124, 2016.

Zhao, M. and Running, S. W.: Drought-induced reduction in global terrestrial net primary production from 2000 through 2009, Science, 329, 940–943, 2010.

Zhu, Z., Bi, J., Pan, Y., Ganguly, S., Anav, A., Xu, L., Samanta, A., Piao, S., Nemani, R. R., and Myneni, R. B.: Global Data Sets of Vegetation Leaf Area Index (LAI)3g and Fraction of Photosynthetically Active Radiation (FPAR)3g Derived from Global Inventory Modeling and Mapping Studies (GIMMS) Normalized Difference Vegetation Index (NDVI3g) for the Period 1981 to 2011, Remote Sensing, 5, 927–948, https://doi.org/10.3390/rs5020927, http://www.mdpi.com/2072-4292/5/2/927, 2013.

https://doi.org/10.5194/bg-2019-212
Preprint. Discussion started: 14 June 2019

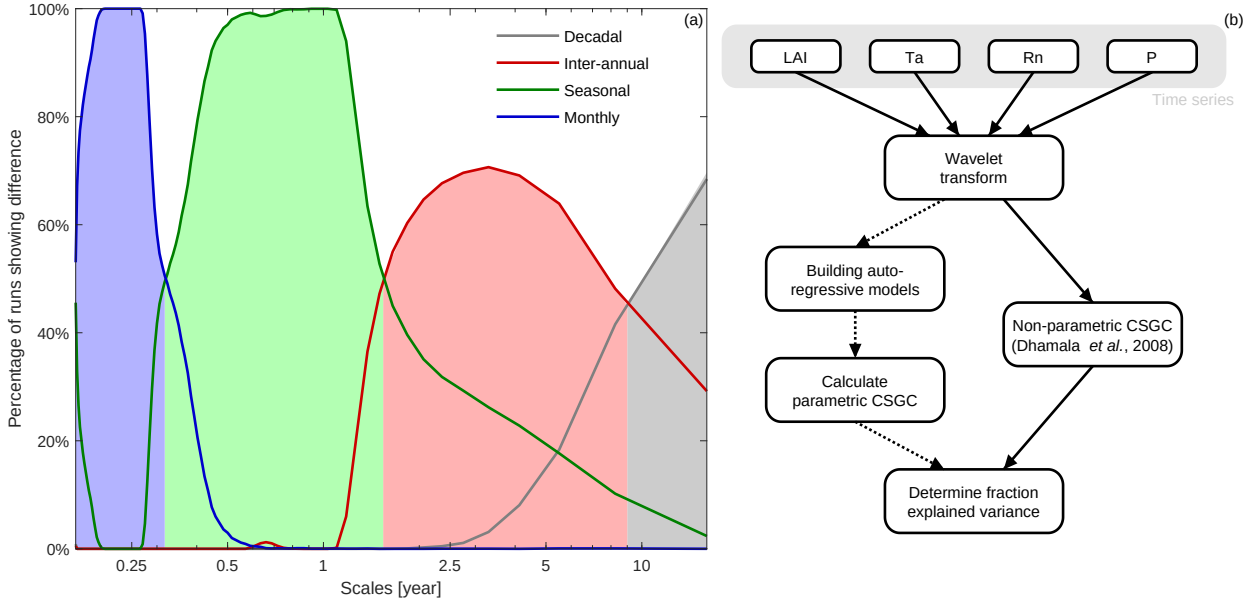

Figure 1. (a) Scales affected by perturbation of variability in synthetic time series at a particular temporal scale. Coloured lines show for each perturbed variability the scales that changed most compared to the unperturbed runs as a percentage of runs out of 100,000. **(b)** Schematic overview of the principle of CSGC, with the extension of calculating the fraction of explained variance.

https://doi.org/10.5194/bg-2019-212
Preprint. Discussion started: 14 June 2019

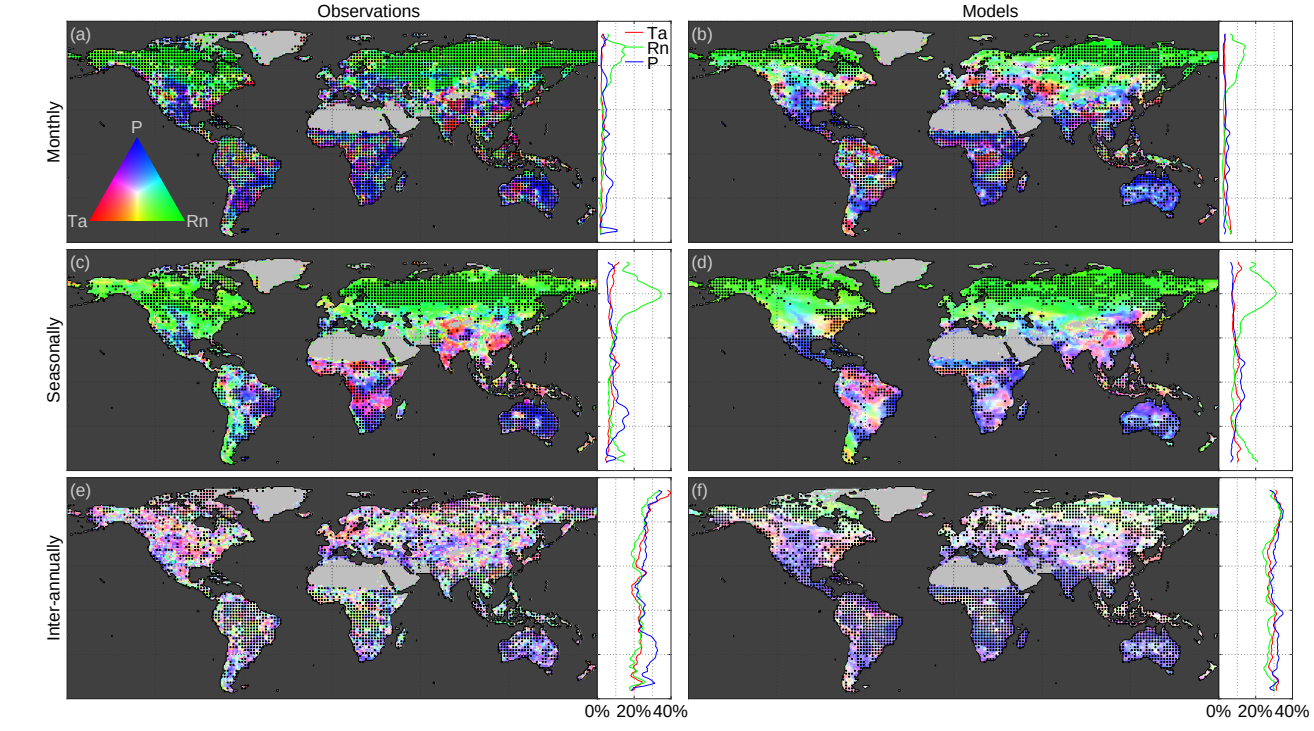

Figure 2. Global climate impact on vegetation. Variability in **(a, c, e)** observed and **(b, d, f)** modelled LAI caused by precipitation (P), air temperature (Ta) and net radiation (Rn) at **(a, b)** monthly, **(c, d)** seasonal, and **(e, f)** inter-annual timescales. Maps show the causality in relative terms with respect to the dominant driver at each pixel, while the latitudinal profiles show the absolute impact of each driver. The period 1982-2015 is taken as reference for the observations, while models span 1956-2005. Modelled maps show the mean from the ensemble of four CMIP5 models: CCSM4, HadGEM2-ES, NorESM1-M, IPSL-CM5A-MR. Dotted pixels indicate a significant (p-value = 1%) primary driver (or at least three models agreeing on the significant primary driver).

https://doi.org/10.5194/bg-2019-212
Preprint. Discussion started: 14 June 2019

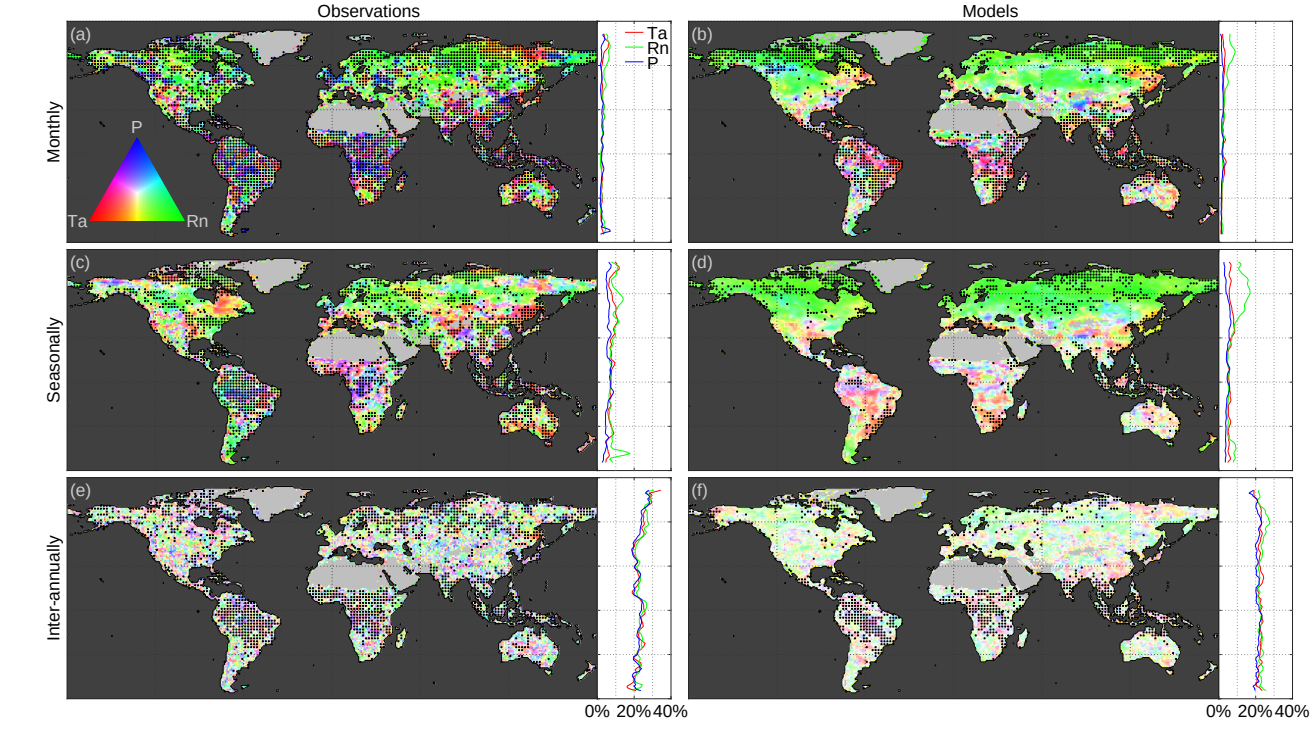

Figure 3. Global vegetation feedback on climate. Variability in precipitation (P), air temperature (Ta) and net radiation (Rn) that is caused by ((**a, c, e**) observed and **(b, d, f)** modelled LAI at **(a, b)** monthly, **(c, d)** seasonal, and **(e, f)** inter-annual timescales. Maps show the causality in relative terms with respect to the strongest feedback at each pixel, while the latitudinal profiles show the absolute feedback on each driver. The period 1982-2015 is taken as reference for the observations, while models span 1956-2005. Modelled maps show the mean from the ensemble of four CMIP5 models: CCSM4, HadGEM2-ES, NorESM1-M, IPSL-CM5A-MR. Dotted pixels indicate a significant (p-value = 1%) strongest feedback (or at least three models agreeing on the significant strongest feedback).

https://doi.org/10.5194/bg-2019-212
Preprint. Discussion started: 14 June 2019

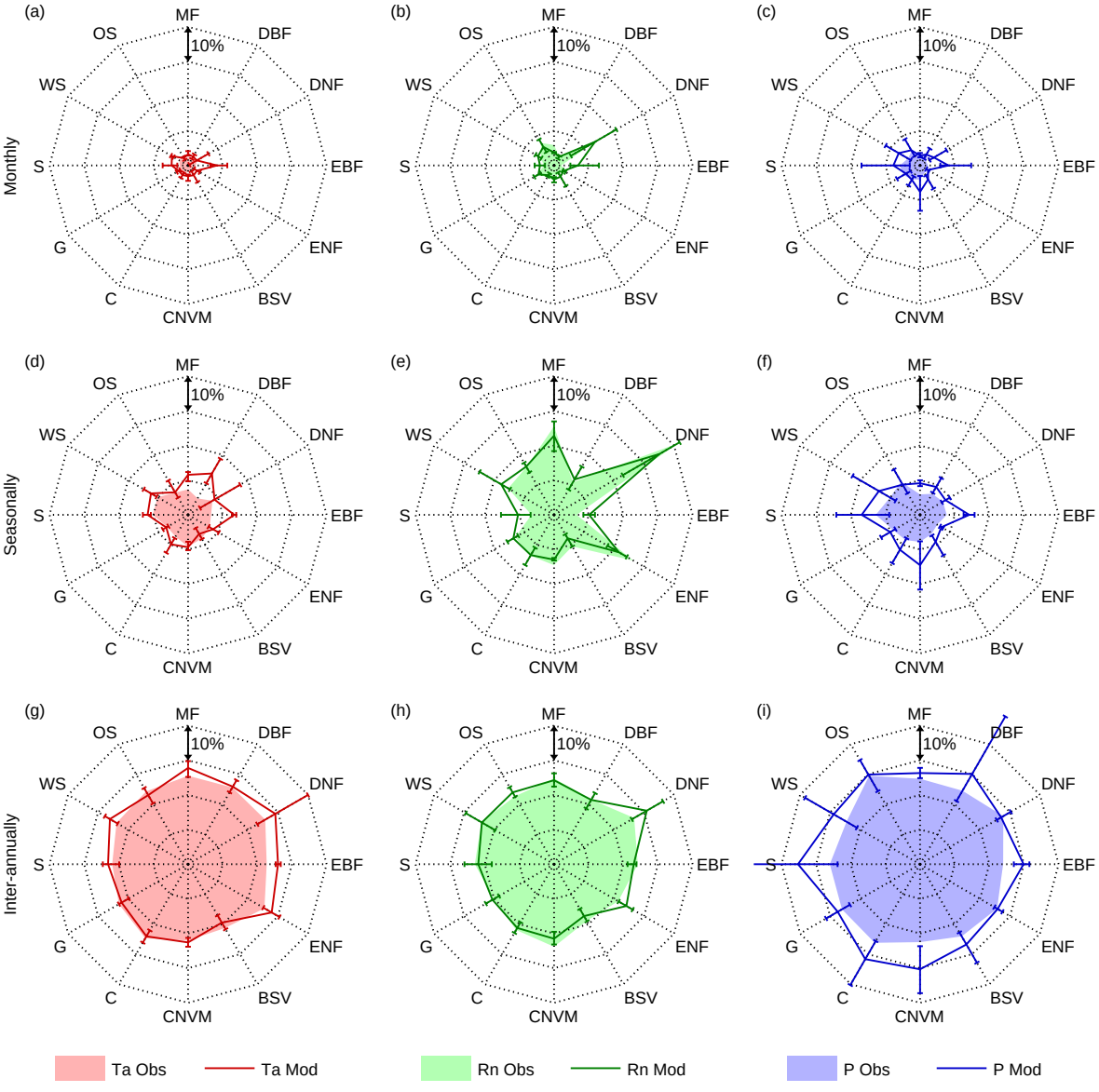

Figure 4. Climate impact on vegetation per biome. Biome averages of absolute observed (filled polygons) and modelled (lines) variation of LAI caused by precipitation (P), air temperature (Ta) and net radiation (Rn), at monthly **(a, b, c)**, seasonal **(d, e, f)**, and inter-annual **(g, h i)** timescales. Models present an error-bar indicating the inter-model maximum, minimum and average results of four CMIP5 models (CCSM4, HadGEM2-ES, NorESM1-M, IPSL-CM5A-MR). Represented biomes are mixed forests (MF), deciduous broadleaf forest (DBF), deciduous needleleaf forest (DNF), evergreen broadleaf forest (EBF), evergreen needleleaf forest (ENF), barren or sparsely vegetated (BSV), cropland or natural vegetation mosaic (CNVM), croplands (C), grasslands (G), savannas (S), woody savannas (WS), and open shrublands (OS).

https://doi.org/10.5194/bg-2019-212
Preprint. Discussion started: 14 June 2019

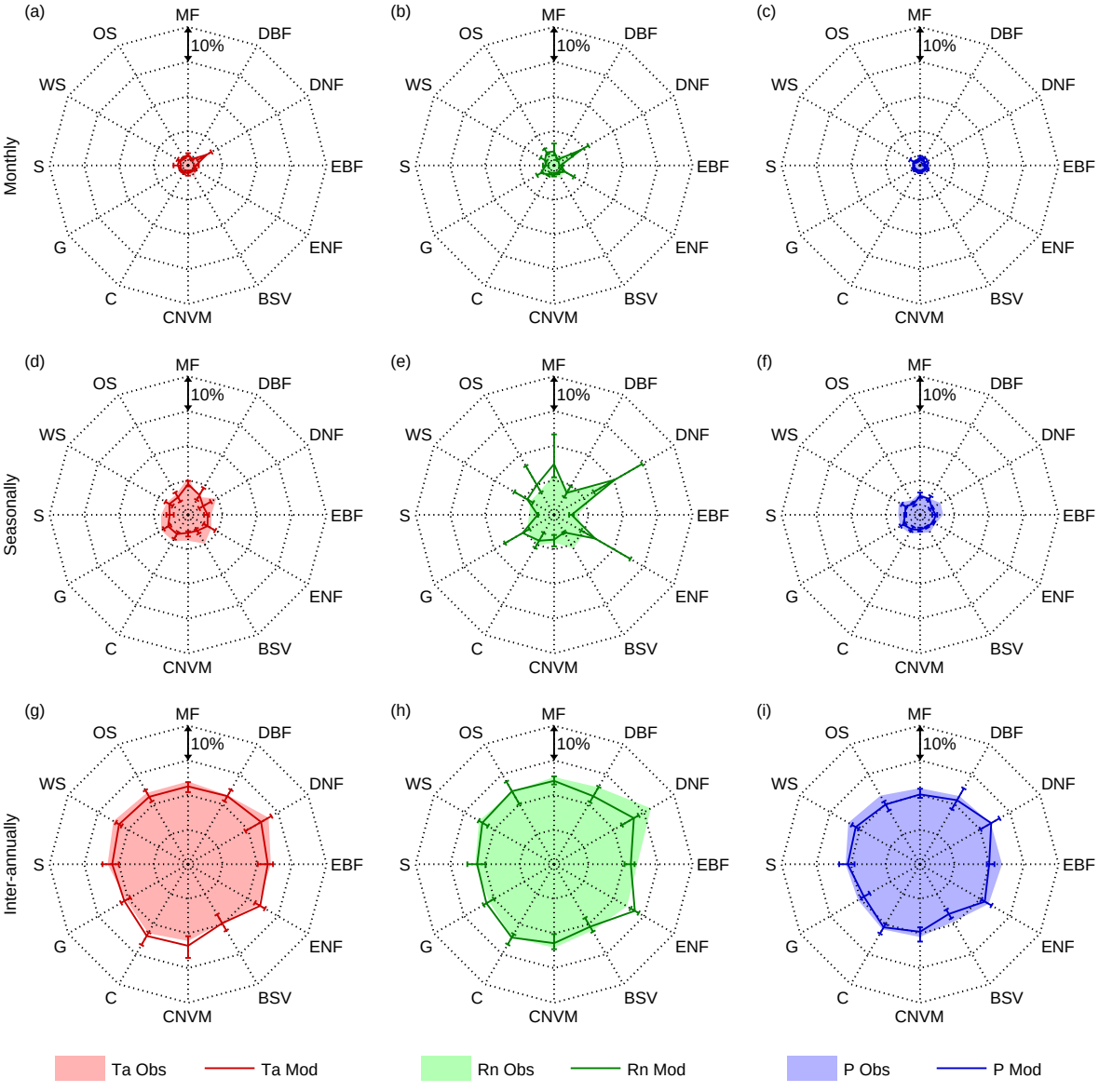

Figure 5. Vegetation feedback on climate per biome. Biome averages of absolute observed (filled polygons) and modelled (lines) variation of precipitation (P), air temperature (Ta) and net radiation (Rn) caused by LAI, at monthly **(a, b, c)**, seasonal **(d, e, f)**, and inter-annual **(g, h i)** timescales. Models present an error-bar indicating the inter-model maximum, minimum and average results of four CMIP5 models (CCSM4, HadGEM2-ES, NorESM1-M, IPSL-CM5A-MR). Represented biomes are mixed forests (MF), deciduous broadleaf forest (DBF), deciduous needleleaf forest (DNF), evergreen broadleaf forest (EBF), evergreen needleleaf forest (ENF), barren or sparsely vegetated (BSV), cropland or natural vegetation mosaic (CNVM), croplands (C), grasslands (G), savannas (S), woody savannas (WS), and open shrublands (OS).

https://doi.org/10.5194/bg-2019-212
Preprint. Discussion started: 14 June 2019

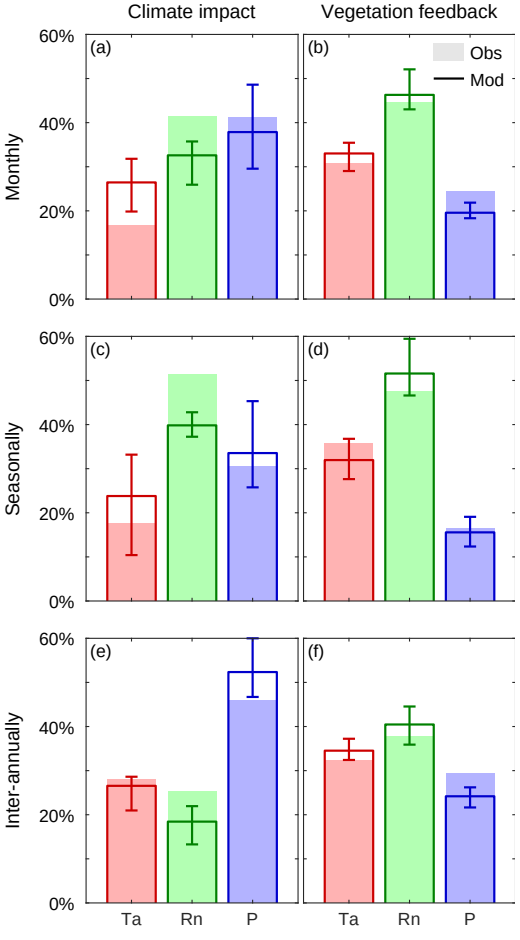

Figure 6. Continental average climate impact on vegetation and vegetation feedback on climate. Continental averages of absolute observed (filled rectangles), and modelled (lines) variation in vegetation **(a, c, e)** (climate **(b, d, f)**) caused by climate (vegetation), at monthly **(a, b)**, seasonal **(c, d)**, and inter-annual **(e, f)** timescales. Models present an error-bar indicating the inter-model maximum, minimum and average results of four CMIP5 models (CCSM4, HadGEM2-ES, NorESM1-M, IPSL-CM5A-MR).

https://doi.org/10.5194/bg-2019-212
Preprint. Discussion started: 14 June 2019

Biogeosciences
Discussions
Open Access
EGU

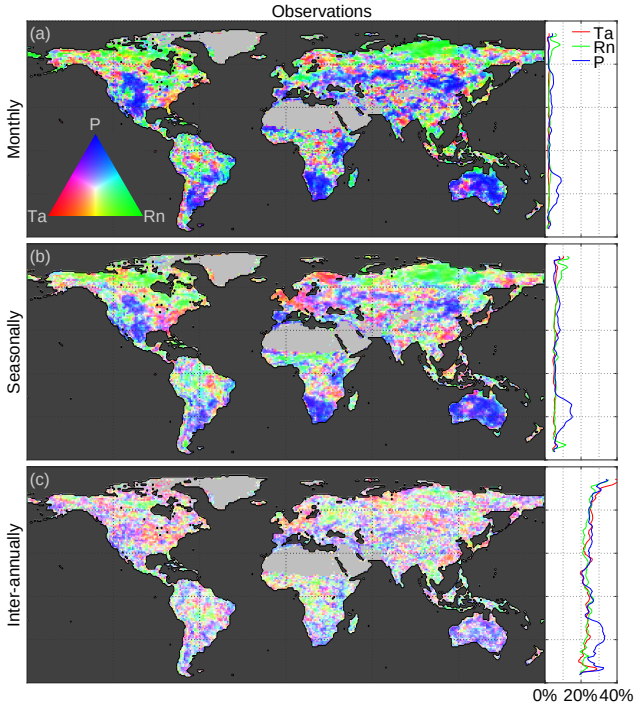

Figure A1. Global climate impact on anomalies of vegetation. Variability in observed anomalies of LAI caused by anomalies in precipitation (P), air temperature (Ta) and net radiation (Rn) at **(a)** monthly, **(b)** seasonal, and **(c)** inter-annual timescales. Maps show the causality in relative terms with respect to the dominant driver at each pixel, while the latitudinal profiles show the absolute impact of each driver. The period 1982-2015 is taken as reference for the observations.

https://doi.org/10.5194/bg-2019-212
Preprint. Discussion started: 14 June 2019

Biogeosciences
Discussions
Open Access
EGU

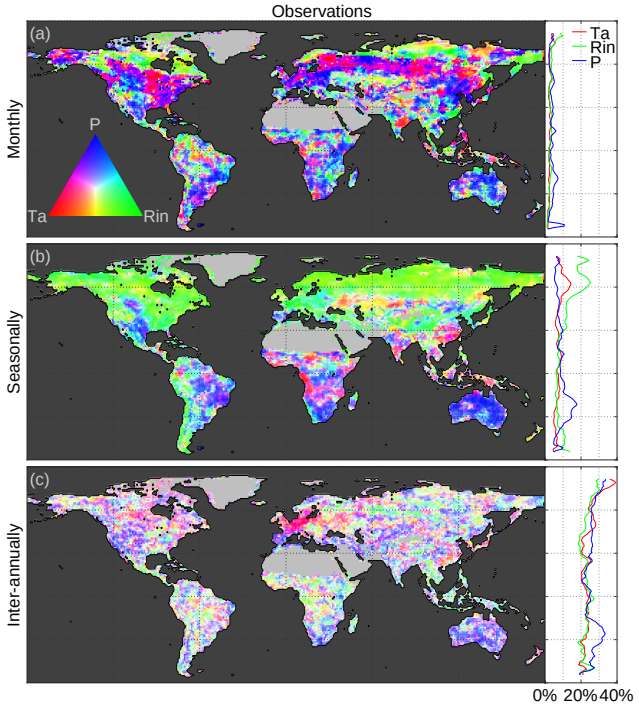

Figure B1. Global climate impact on vegetation using incoming radiation instead of net radiation. Variability in observed LAI caused by precipitation (P), air temperature (Ta) and incoming radiation (Rin) at **(a)** monthly, **(b)** seasonal, and **(c)** inter-annual timescales. Maps show the causality in relative terms with respect to the dominant driver at each pixel, while the latitudinal profiles show the absolute impact of each driver. The period 1982-2015 is taken as reference for the observations.

https://doi.org/10.5194/bg-2019-212
Preprint. Discussion started: 14 June 2019

Biogeosciences
Discussions
Open Access
EGU

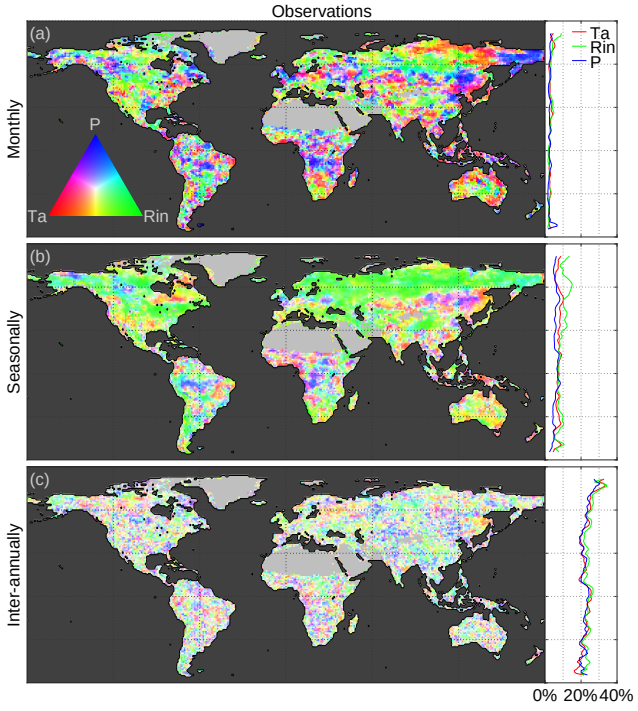

Figure C1. Global vegetation feedback on climate using incoming radiation instead of net radiation. Variability in precipitation (P), air temperature (Ta) and incoming radiation (Rin) that is caused by observed LAI at **(a)** monthly, **(b)** seasonal, and **(c)** inter-annual timescales. Maps show the causality in relative terms with respect to the strongest feedback at each pixel, while the latitudinal profiles show the absolute feedback on each driver. The period 1982-2015 is taken as reference for the observations.